© 2016

Niloy Talukder

ALL RIGHTS RESERVED

DESIGN OF ANALOG FRONT-END CIRCUITRY WITH DRIFT REMOVAL AND GAIN ENHANCEMENT FOR A HIGHLY SENSITIVE HANDHELD IMPEDANCE CYTOMETER

By

NILOY TALUKDER

A thesis submitted to the

Graduate School-New Brunswick

Rutgers, the State University of New Jersey

In partial fulfillment of the requirements

For the degree of

Master of Science

Graduate Program in Electrical and Computer Engineering

Written under the direction of

Mehdi Javanmard

And approved by

____

____

____

New Brunswick, New Jersey

October 2016

ABSTRACT OF THE THESIS

Design of Analog Front-End Circuitry with Drift Removal and Gain Enhancement for a Highly Sensitive Handheld Impedance Cytometer

by

NILOY TALUKDER

Thesis Director:

Mehdi Javanmard

We present a portable system for personalized blood cell counting consisting of a microfluidic impedance cytometer with portable analog readout feeding into an analog-to-digital converter (ADC). The novel design of the analog readout, which consists of a lock-in-amplifier followed by a high-pass filter stage for subtraction of drift and DC offset, and a post-subtraction high gain stage, enables detection of particles and cells as small as 1 μm in diameter, despite using a low-end 8 bit ADC. Applications such as personalized health monitoring require robust device operation and resilience to clogging, thus it is desirable to avoid using channels comparable in size to the particles being detected, thus requiring high levels of sensitivity. Despite using low-end off-the-shelf hardware, our sensing platform was capable of detecting changes in impedance as small as 0.032%, allowing detection of 3 μm diameter particles in 300 μm wide channel. The consecutive upward and

downward signature of recorded peaks further helps to differentiate the signal from the noise floor. The performance of our system is comparable to that of a high-end bench-top impedance spectrometer under experimental condition. The novel analog design allowed for an instrument with a footprint of less than 80 cm^2. The aim of this work was to demonstrate the potential of using microfluidic impedance spectroscopy for low-cost health monitoring. We demonstrated the utility of the platform technology towards cell counting, however our platform is broadly applicable to assaying wide panels of biomarkers including proteins, nucleic acids, and various cell types.

ACKNOWLEDGMENTS

First and foremost, I would like to thank my advisor Dr. Mehdi Javanmard for his valuable guidance and supervision throughout my Master's research program. I am really grateful to Dr. Michael Caggiano and Dr. Yicheng Lu for serving on my Master's thesis committee and for their evaluation on my thesis research work. Without their direction, I would not have been able to complete my master's thesis.

I would like to thank all my lab partners, especially, Pengfei Xie, Zhongtian Lin, Tuan Le and Azam Gholizadeh for their persistent help with sensor fabrication and experiments. I am greateful to Abbas Furniturewalla for assisting me with experiments and contributing in my circuit design.

And last but not the least, I would like to thank my parents and my siblings for helping me at every stage of my life. Without their tremendous support and sacrifice I would not have been able to come up to this point in my career.

TABLE OF CONTENTS

LIST OF TABLES

LIST OF FIGURES

CHAPTER 1

INTRODUCTION

1.1 Flow Cytometry and Portable Medical Device

Flow cytometry, which is the gold standard technique for cell counting is primarily based on optical detection of fluorescently labeled biological cells and particles suspended in a stream of fluid. It requires bulky and costly optical instrumentation and also laborious fluorescent tagging of cells [1]. Impedance cytometry, which is based on electrical detection, is advantageous over optical readout because of the potential for developing instrumentation with a small footprint. Electrical impedance cytometry can be used towards detection of proteins, cells, and nucleic acids with high specificity and sensitivity [2]. Significant improvements in wireless technology has also made it possible for hand-held medical devices to wirelessly connect with miniaturized computing devices like smart phones and tablets, thus making results readily available for both the patient and medical professionals. The wireless coupling of lab-on-a-chip electronic biosensors with smart phones can enable continuous monitoring of patient health [3] - [4].

The ability to detect single cells and particles at the micro-scale generally requires a highly sensitive system that can detect at least 0.1% change in baseline impedance. This typically requires both high-end analog-to-digital conversion hardware and also channel sizes comparable to the particle being detected. Small channel sizes generally result in device failure due to clogging of the microfluidic channels, and high-resolution analog to digital converters usually require either a customized integrated circuit or a data acquisition card that plugs into a notebook or personal computer. To be able to detect single particles robustly without clogging channels, requires a sensor cross-sectional area five to ten times larger than the largest particle that will be detected, which is difficult to achieve with low-resolution off-the-shelf analog-to-digital converters. We developed analog-front-end circuitry for a microfluidic impedance cytometer with improved sensitivity allowing for the use of low-resolution (8-bit) ADC for data acquisition.

1.2 Lock-in-amplification (LIA) Technique and Previous Works

One of the major challenges of electrical impedance detection is detecting low signal-to-noise ratio (SNR) output signals provided by low voltage, low power sensors, which can be an order of magnitude smaller than electrical noise and interference signals from the environment [5]. One of the most common techniques for detecting very small AC signals down to a few nano-volts is lock-in-amplification (LIA), which makes use of the synchronous phase sensitive detection (PSD) technique. This is significant as it promises the sensitivity required to detect these small output signals. When a narrow bandwidth around the modulation reference frequency is allowed to pass through to the output, the remaining signal is filtered out, allowing a signal which is a thousand times weaker than the noise environment can be successfully detected [6]. The utility of the lock-in-amplifier has been demonstrated in various electronic sensing systems including contactless conductivity detection for microchip-based capillary electrophoresis (CE) (Lichtenberg et al.), where a synchronous detector phase readout circuit was used [7]. In the synchronous detection architecture much care needs to be taken for perfect matching of the frequency and phase values of the data with the reference signal, otherwise, the signal cannot be completely recovered. Gabal et al. has shown the use of two parallel PSD to eliminate system phase dependence [8]. Recently, Marcellis et al. presented a LIA chip that performs automatic alignment of the relative phase between the input and the reference signal and performs self-tuning [9]. Also, using a high-frequency modulation reference signal for impedance spectroscopy shorts out the capacitive coupling in the sensor, and thus the output signal can be linearly amplified and detected using the LIA technique. The upper frequency of the reference signal is limited by the sampling rate of the data acquisition system which has to be more than twice of the upper frequency of the reference signal according to Nyquist rate [10]. For a LIA, a multiplier is used to demodulate the carrier and peak frequency to baseband and a low pass filter is used to detect a low-frequency sensor signal and filter out a high-frequency signal and noise. The LIA can be of analog or digital architecture or both. The digital LIA has gained popularity as it is suitable for multi-frequency operation [10]–[15], hence commercial lock-in-amplifiers often use a digital architecture [16]–[17]. However, to develop a portable hand-held LIA, where single frequency excitation is sufficient, the use of a costly and bulky digital architecture is excessive. Also, digitizing the analog output of the sensor, which is a small peak carried on a baseline signal which drifts randomly with time, requires a very high resolution and high-end analog-to-digital converter. In the literature various analog LIA chip architectures have been presented including designs using a single supply, a decrease in supply voltage, power consumption, a reduction in chip area, and exploitation of new architectures to improve performance [18]–[29]. Various integrated LIA chips have been developed with a power consumption as low as 207.7 μW [29] and areas as small as 0.013 mm^2 [28]. A fully analog readout circuit is thus a suitable solution for miniaturized integrated portable medical devices.

1.3 Statement of the Problem

Normally, a high precision benchtop commercial grade digital LIA is used in the research laboratories for measuring the signal coming out of an impedance cytometer. But such LIA instrument is bulky and very costly which makes it unsuitable for use in portable medical device. Our research problem was to work on reducing the size and cost of the readout circuit. This would allow us to design a palm-size portable medical device which can provide the high precision required to detect small near sub-micron bead flowing in the microfluidic channel.

1.4 Objective and Approach

For our application we needed to detect a very low strength analog signal coming out of the microfluidic impedance cytometer. This signal was time varying in nature due to signal drift introduced by the base solution. We needed a high precision DAQ system to digitize the time varying signal which requires complex architecture involving a large size and a high cost. But our focus was to reduce cost while designing the readout circuit for the portable medical device. The signal was also buried in noise which was introduced by the sensor, the readout circuit, the Data Acquisition (DAQ) device, and the environmental interference noise. For noise reduction, the ideal approach is to use low noise integrated circuits to build the readout circuit, and careful layout design.

Since we were in the beginning stage, the focus was not on power supply voltage reduction, power consumption reduction or extensive noise minimization in the circuit design. All of these will be explored in later works. For our design of the analog readout circuit, we focused on using low-cost circuit components which are not optimized for minimum noise performance. We worked on designing a simple but effective layout design that provides cross-talk noise removal and smooth signal propagation through the circuit. For our setup we did not need information of the input reference frequency. So, we used a high pass filter to remove the DC baseline of the signal. Then high gain stages are utilized to bring the low-strength signal out from the system noise. Lastly, we replaced the recording DAQ system with ATMega328p microcontroller chip from the handheld Arduino Uno Rev3 board which could successfully digitize the output signal while maintaining high resolution.

1.5 Organization of Thesis

The thesis is organized as follows. In chapter 2, we discussed the proposed novel architecture of the readout circuit for the microfluidic-based impedance cytometer. We also presented an analytical noise model of the circuit and the noise simulation results. Based on the noise calculation, the SNR is predicted. We presented the implemented circuit on the PCB and noise measurement on the circuit in chapter 3. The results from the cytometry experiment and their analysis are presented in chapter 4. We further explored results from the 3µm diameter bead experiment with an Arduino low-resolution ADC in chapter 5. Finally, in chapter 6, the thesis is concluded summarizing all the findings.

CHAPTER 2

NOVEL ANALOG FRONT-END CIRCUITRY

2.1 Lock-in Amplification Principle

The traditional LIA consists of a reference frequency generator, a trans-impedance amplifier, a mixer, and a low-pass filter stage. Experiments have shown that for the frequency region between 100 kHz and 1 MHz, impedance is dominated by bulk solution resistance across the electrolyte. Above a frequency of 1 MHz, there is a drop in impedance due to capacitance of the cell membrane [1], thus for simple cell counting and sizing, we choose to operate at a reference frequency signal of 500 kHz. The modulated current signal coming out of the sensor is converted into a voltage signal using a trans-impedance amplifier. Then a mixer stage demodulates the voltage signal by multiplying it with the input frequency signal. The demodulated signal is then passed through a low pass filter stage with a low cut-off frequency so that only the signal peak of interest gets passed. In addition to the input frequency, high-frequency noise components are filtered out which improves SNR of the system. The low pass filter cut-off frequency is determined based on the transit time of the bead between two electrodes.

2.2 Proposed Additions to LIA Design for Application in Microfluidic Impedance Cytometry

Since we are only interested in AC signal variation corresponding to particle/cell flow in the sensor, a DC blocking capacitor is used to remove the DC baseline introduced by the carrier frequency. By implementing this high-pass filtering in the analog domain, we now have the ability to apply a large gain so that the magnitude of the peak is detectable by a low-resolution ADC. Thus, two high gain stages are used to amplify the output AC signal from the low pass filter. The high gain stage also amplifies the noise level of the system; however, the signal peak dominates over the noise. The output of the low pass filter is:

$$V_{LPF} = \frac{1}{2} V_{TIA} V_{sig} [1 + mx(t)] \cos \Theta_{sig} \quad \text{...} \quad (1)$$

where, V_{TIA} and V_{sig} are the amplitudes of the output of the trans-impedance amplifier and the input reference signal respectively, $mx(t)$ is a time varying component introduced by particle/cells flowing through the electrode sensor, and Θ_{sig} is the phase of the input signal. At the output of the DC blocking capacitor, we obtain

$$v_{cap} = \frac{1}{2} V_{TIA} V_{in} mx(t) \cos \Theta_{sig} \quad \text{...} \quad (2)$$

Thus, the output signal does not depend on the phase matching between the reference signal and the current coming out of the sensor. The concept of this lock-in-amplification based resistive biosensor is illustrated in Fig. 2.1. While designing the analog front-end circuit which operates at a high frequency, we considered several factors for minimizing noise and interference including power supply noise reduction and minimization of output

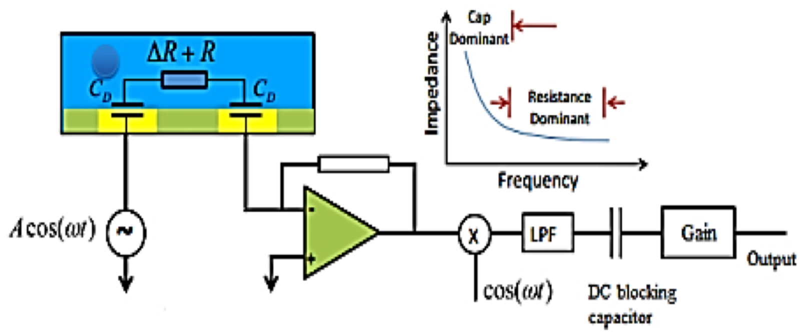

Fig. 2.1 Schematic of lock-in-amplification based resistive biosensor.

voltage fluctuations, and other important considerations necessary when including frequency generation on-board (details explained in appendix section).

2.3 Analytical Noise Model and Noise Simulation

In order to develop a design space to understand the key performance parameters, we calculated and simulated (using LTSpice software) the total noise of the system considering all of the major sources of noise. We did so by calculating the output referred voltage noise. We compared this calculation with the noise simulation results of the system circuit model. Fig. 2.2 illustrates the noise model of the circuit.

The calculation of the output referred voltage noise of the circuit is presented here. The output voltage noise of the trans-impedance amplification stage is:

$$E_{n1}{}^2 = \left(R_{f1}/R_{biosensor}\right)^2\left(V_{biosensor}{}^2 + V_{n1}{}^2\right) + R_{f1}{}^2 i_{n1}{}^2 + V_{f1}{}^2 \qquad \ldots\ldots\ldots.. \quad (3)$$

The output voltage noise of the mixer stage is:

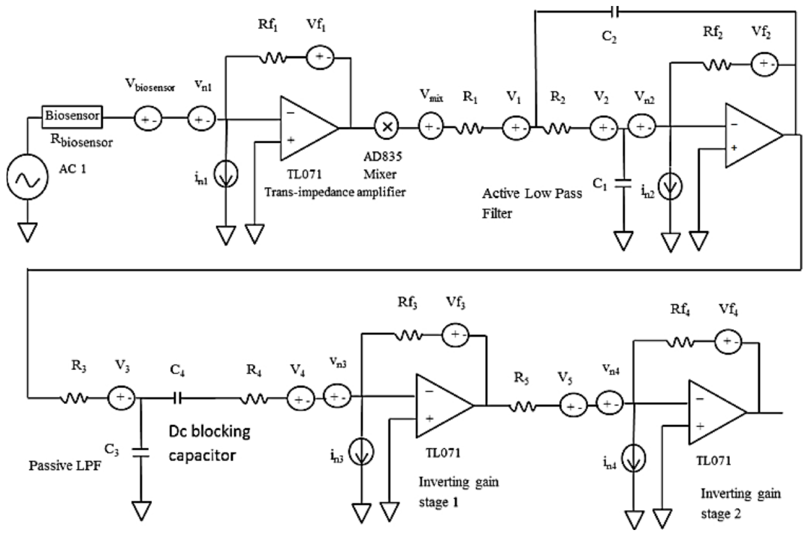

Fig. 2.2 Noise model of the readout circuit

$$E_{n2}{}^2 = E_{n1}{}^2 + V_{mix}{}^2 \quad \ldots\ldots\ldots\ldots \quad (4)$$

The output voltage noise of the active low pass filter stage is:

$$E_{n3}{}^2 = \left(Z_{c1}/(R_1 + R_2||Z_{c2} + Z_{c1})\right)^2 (E_{n2}{}^2 + V_1{}^2) + Z_{c1}{}^2 \left(\left(\begin{vmatrix} V_2 & -R_2 \\ -V_2 & R_2 + Z_{c2} \end{vmatrix} / \begin{vmatrix} R_1 + R_2 + Z_{c1} & -R_2 \\ -R_2 & R_2 + Z_{c2} \end{vmatrix} \right)^2 + \left(\begin{vmatrix} V_{n2} & -R_2 \\ -V_{n2} & R_2 + Z_{c2} \end{vmatrix} / \begin{vmatrix} R_1 + R_2 + Z_{c1} & -R_2 \\ -R_2 & R_2 + Z_{c2} \end{vmatrix} \right)^2 \right) +$$

$$i_{n2}{}^2 \left[\left((R_1 + R_2||Z_{c2})Z_{c1} \right) / (R_1 + R_2||Z_{c2} + Z_{c1}) \right]^2 + \left(V_{f2} + Z_{c1} \left(\begin{vmatrix} R_2 + Z_{c2} & V_{f2} \\ -R_2 & 0 \end{vmatrix} / \begin{vmatrix} R_2 + Z_{c2} & -R_2 \\ -R_2 & R_1 + R_2 + Z_{c1} \end{vmatrix} \right) \right)^2 \quad \ldots\ldots\ldots\ldots \quad (5)$$

The output voltage noise of the cascaded passive low pass filter and DC blocking capacitor is:

$$E_{n4}{}^2 = \left((E_{n3} - V_3)/(R_3 + Z_{c3}) \right)^2 Z_{c3}{}^2 \quad \ldots\ldots\ldots\ldots \quad (6)$$

The output voltage noise of the first inverting gain stage is:

$$E_{n5}{}^2 = \left(R_{f3}/R_4\right)^2\left(V_4{}^2 + V_{n3}{}^2 + E_{n4}{}^2\right) + R_{f3}{}^2 i_{n3}{}^2 + V_{f3}{}^2 \quad \text{(7)}$$

Finally, the output voltage noise of the second inverting gain stage is:

$$E_{n6}{}^2 = \left(R_{f4}/R_5\right)^2\left(V_5{}^2 + V_{n4}{}^2 + E_{n5}{}^2\right) + R_{f4}{}^2 i_{n4}{}^2 + V_{f4}{}^2 \quad \text{(8)}$$

Here, the variables are presented in Fig. 2.2. V_n and i_n correspond to the input referred voltage and current noise of the operational amplifier and they are numbered according to their order in the circuit. Each resistor is also modeled as a thermal voltage source. The capacitors do not serve as independent noise sources.

The circuit was also simulated using LTSpice IV simulation software. The simulation result closely matches with the theoretical calculation. The output voltage noise frequency spectrum simulation of the circuit in LTSpice is shown in Fig. 2.3. The inclusion of two

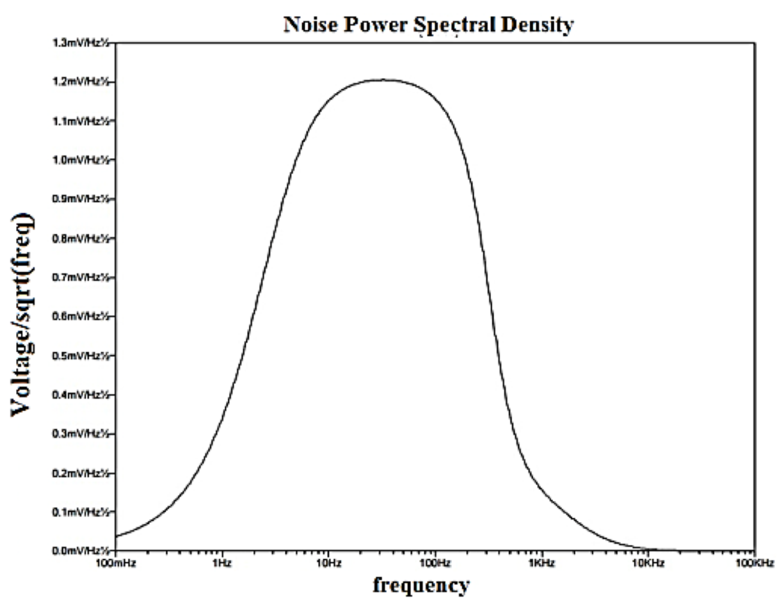

Fig. 2.3 Noise simulation of the readout circuit

high gain stages increase the noise to 1.2 mV/√Hz within the period of frequency 10 Hz and 100 Hz. The total estimated RMS noise value from the simulation is 26.127 mV.

2.4 SNR Prediction

The lock-in amplification process is simulated in MATLAB to estimate the SNR. For simulation, the following parameters are used:

In the microfluidic channel,

- electrode width = 10 µm,
- electrode separation = 15 µm.
- Number of electrode fingers = 2.
- Fluid flow rate = 0.08 µl/min.
- Channel width = 30 µm.

Target particle diameter size is varied from 100 nm to 10 µm with a 100 nm step. NaCl is considered as a base electrolyte fluid.

The microfluidic-based biosensor model is shown in Fig. 2.4.

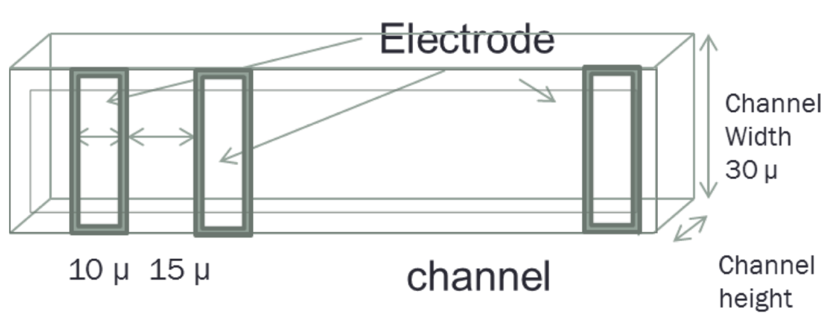

Fig. 2.4 Microfluidic biosensor model

The resistance of the base solution is calculated using the elliptical model of current conduction from Gerwen et al. [30]. The design flow in MATLAB is shown in Fig. 2.5. The simulation plot is shown in Fig. 2.6. In Fig. 2.7 particle diameter is taken up to 3 µm.

Calculation of current variation caused by bead flow in the channel

⇩

Adding thermal current noise introduced in the microfluidic channel

⇩

Multiplying with trans-impedance gain to get voltage signal

⇩

Multiplying with gain of 100,000 introduced by two high gain stages

⇩

Adding theoretical noise calculated for lock-in-amplifier design

⇩

Determining mean of baseline

⇩

Finding peak of complete signal and noise variation

⇩

SNR

Fig. 2.5 MATLAB Design Flow

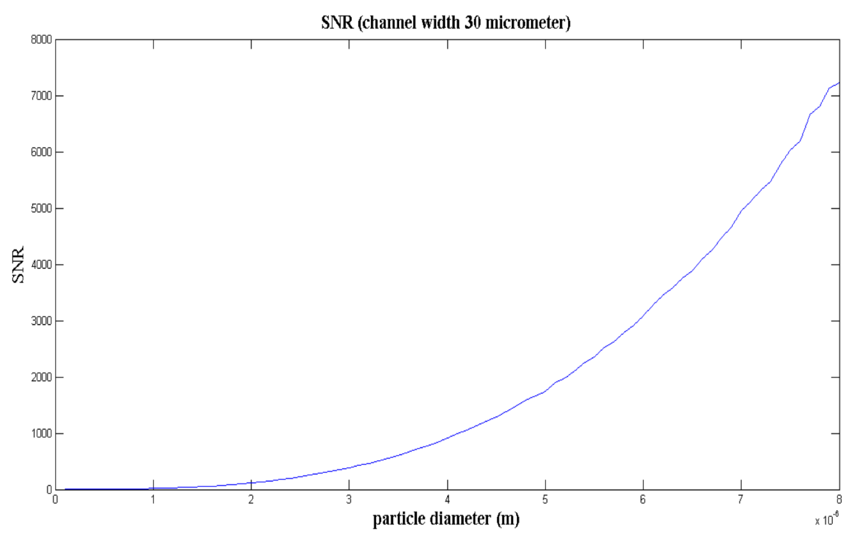

Fig. 2.6 Signal to noise ratio (SNR) calculation varying bead diameter from 100 nm to 10 µm flowing in a 30 µm wide channel.

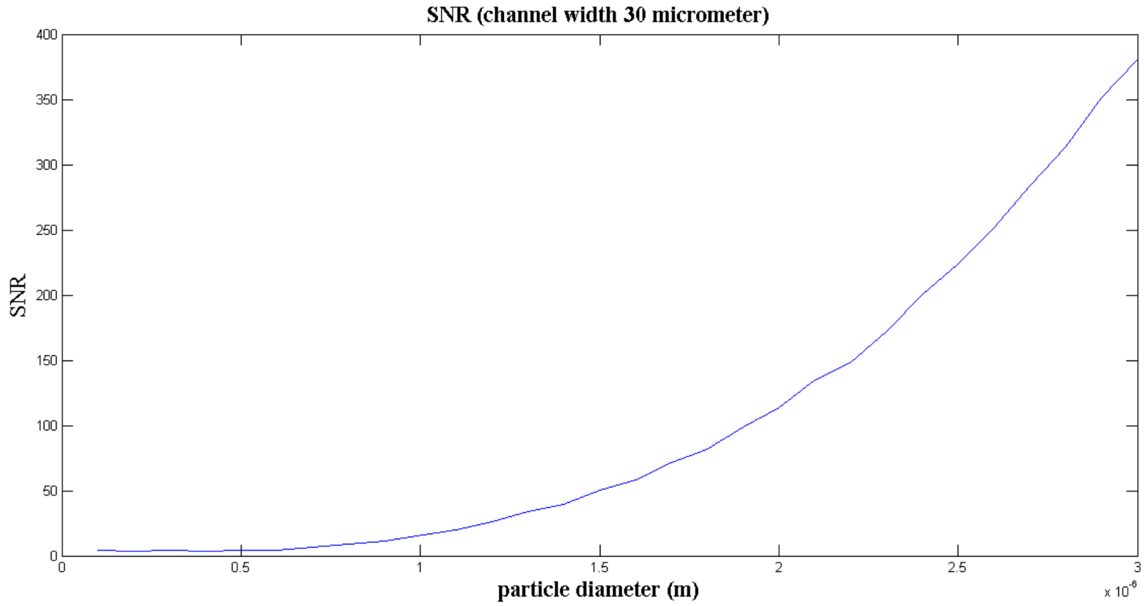

Fig. 2.7 SNR calculation varying bead diameter from 100 nm to 3 µm flowing in a 30 µm wide channel.

Table 1 below presents the theoretical SNR prediction for the beads used during the experiment.

TABLE 5.1: THEORETICAL SNR PREDICTION

Channel width (µm)	Bead diameter (µm)		
	1	3	8
30	15.71	391.5	7373

An elliptical model for base electrolyte solution resistance approximation is presented in appendix 7.1. We calculated the increase in resistance of the conducting channel due to bead flow through the active sensing pore. Our calculation is based on Deblois and Bean circular cylindrical model which is explored in appendix 7.2. The formula that is used to calculate the SNR is presented in appendix 7.3.

CHAPTER 3

PRINTED CIRCUIT BOARD (PCB) IMPLEMENTATION AND DATA ACQUISITION

3.1 Circuit Description

The LIA design was tested on a breadboard first and then implemented on the PCB as shown in Fig. 3.1. Two (EBL 6F22 9V 600 mAh lithium ion rechargeable) batteries are used as the power supply. There is a DPDT toggle switch to turn the batteries on and off. The batteries can supply power for approximately 12 hours. Two voltage regulators (LT1763 and LT1964 from Linear Technology) are used to deliver +5V and -5V

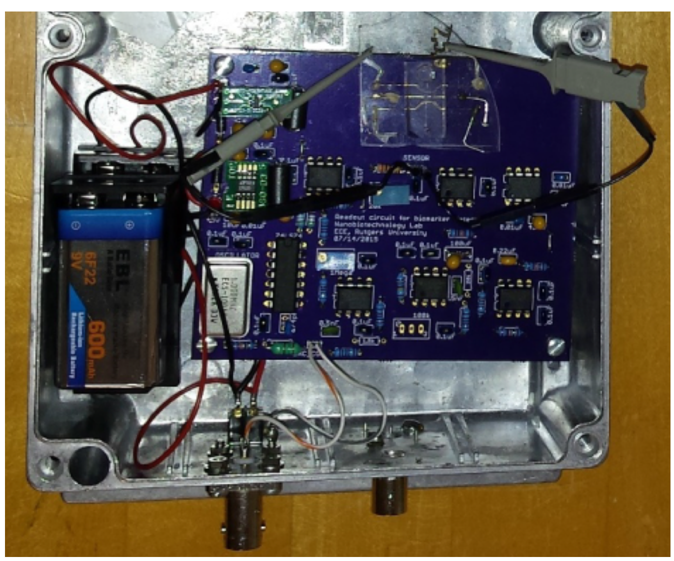

Fig. 3.1 Printed circuit board with the biochip

respectively from the 9V batteries. On the printed circuit board, we have implemented a power supply bypassing technique for both high and low-frequency noise rejection. Two electrode pads from the biochip are connected to the readout circuit through clips. A relatively high frequency (500 kHz) 2 Volt Peak-to-Peak (V_{p-p}) input signal is generated on board from a 1 MHz crystal oscillator ECS-100AC and a passive LC tank and then fed into the biosensor. The higher the amplitude of the input signal, the higher the SNR will be. We used a 2 V_{p-p} signal so that the dc offset of the subsequent stages do not bring the signal to rail and clip it. The input signal has a resolution of 20 mV and the spectrum of the bandpass passive LC filter tank is shown in appendix 7.5.3. The center of the band is at 500 kHz so it rejects all other frequencies and gives a smooth sine wave signal. The AC signal goes into the biochip through one electrode pad and the output current from the biochip is collected through the other electrode pad. In Fig. 3.2 a schematic of the biosensor and connection to the circuit is shown.

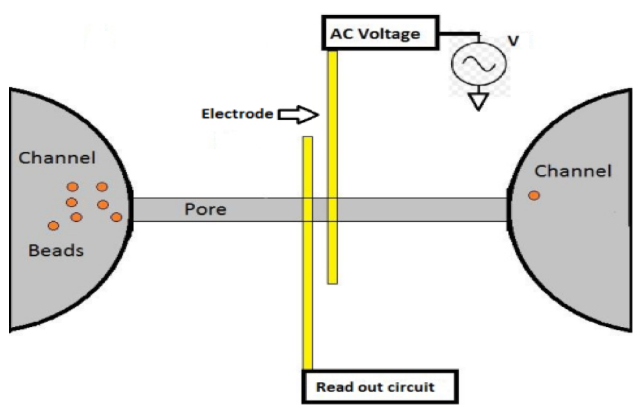

Fig 3.2. Schematic of the biosensor and connection to the readout circuit

To implement the trans-impedance stage, a low-noise operational amplifier (TL071CP from Texas Instruments) was used. In the feedback path, a 20 kΩ potentiometer is used alongside a 2 kΩ resistor to control the trans-impedance gain. So, the trans-impedance gain is between 0.04 to 0.44. The mixer stage is implemented using a four quadrant multiplier (AD835 from Analog Devices). A 3rd order Butterworth low pass filter (cut off 100 Hz) is implemented using the same low noise operational amplifier TL071CP. This filter gives a 60 dB roll off per decade and rejects high-frequency noise. We have used a DC blocking capacitor as high pass filter to remove the baseline of the signal.

At the final stage of the circuit, two inverting high gain stages are used to amplify the detected peak from the biosensor. The first inverting stage has a gain of 1000. The second inverting stage has a potentiometer for adjustable gain between 100 and 1100. So, we can achieve a gain as high as 1.1 MV/Amp. The potentiometer was set to a minimum during the experiment so the net gain was 10^5. In the PCB, we used a two-layer ground plane to reduce crosstalk between wires and made sure there was no potential difference between the ground connections of the different circuit elements. Various techniques have been presented in the past for removing electro-magnetic interference in PCBs [31]. The full footprint of our printed circuit board was 10 cm x 8 cm.

3.2 Data Acquisition

In this work, we utilized two different techniques for data acquisition. Initially, we tested and characterized the circuit and system using a benchtop system, a Labview (National Instruments, TX, USA) data acquisition card and a desktop computer. After fully verifying system performance, we replaced the Labview data acquisition system with miniaturized handheld microcontroller.

For the initial desktop data acquisition system, a BNC (Bayonet Neill–Concelman) cable was used to collect the output signal of the readout circuit. The analog output of the readout circuit was converted to a digital signal using a multipurpose data acquisition card (National Instruments RIO USB 7856R). The output voltage signal was reconstructed and post-processed using Labview software. The recorded data was processed in MATLAB 2012a (Mathworks Inc.). Later we replaced the desktop data acquisition system with the Atmega 328p, a microcontroller from the handheld Arduino Uno Rev3 board (ARDUINO.CC). In order to increase the sampling frequency on the Arduino, only the LO register of the microcontroller was used, and the HI register was omitted, resulting in only 8-bit resolution. Because the input of the Arduino cannot sample negative voltages, the output of the LIA was biased to a positive voltage range, using a simple voltage divider and another regulated external power source. The 8-bit resolution ADC was sufficient to digitally reconstruct the measured analog signal. The output digital signal coming out of the Arduino board was reconstructed using Arduino 1.6.3 software and then recorded using Processing 3 software (processing.org). The recorded data was then processed in MATLAB 2012a (Mathworks Inc.) to reduce noise and quantify peaks corresponding to each bead flow. The block diagram of the experimental setup is illustrated in Fig. 3.3. In appendix 7.5, circuits for different blocks are elaborately presented and different design considerations are discussed. Also, LTSpice simulation files and layout design files are presented.

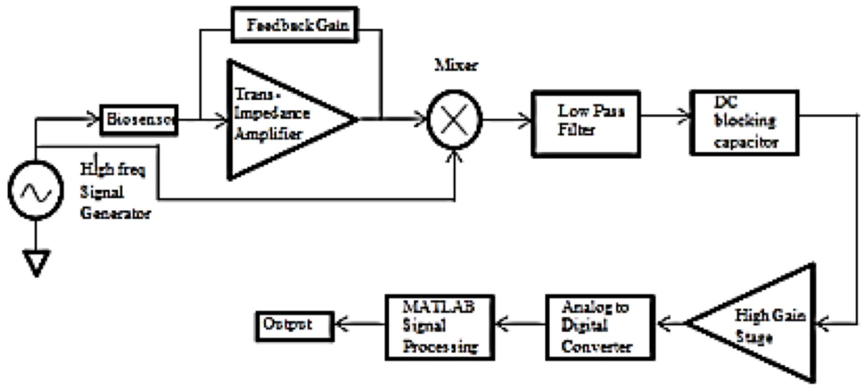

Fig. 3.3 System block diagram

3.3 Noise Measurement

We experimentally proceeded to determine which source of noise dominates the system. We measured the noise power spectral density by grounding the input of the circuit. We individually isolated each component in the circuit to characterize its contribution to the entire noise output. We measured the noise level of the circuit for the following five cases: 1) The PCB with no biosensor connected. 2) The PCB connected to the biosensor but no fluid in it. 3) The PCB with a 50 kΩ resistor in place of the biosensor. 4) The PCB and the biosensor with fluid and beads in it. 5) The DAQ card input shorted to measure its noise levels. The measurement results are overlaid in Fig. 3.4. From this figure, it is seen that noise from the first four cases dominates over the DAQ card noise. The low-frequency flicker noise comes from the DAQ card and contributes to the PCB noise. The PCB noise with the 50 kΩ resistor is similar to the noise of the PCB with the biosensor, so a 50 kΩ resistor is used in the noise simulation in place of the biosensor.

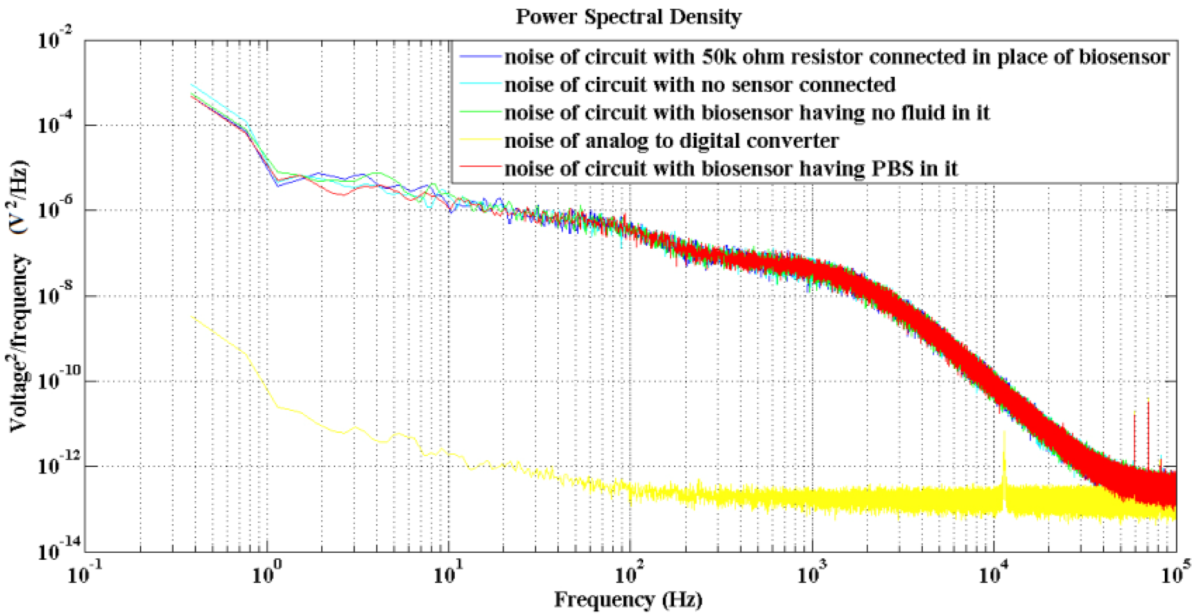

Fig. 3.4 Noise power spectral density for 1) The PCB with no biosensor connected, 2)The PCB connected to the biosensor but no fluid in it, 3) The PCB wth 50 kilo ohm resistor in place of biosensor, 4)The PCB and biosensor with fluid and beads in it, 5)The DAQ card input shorted to measure its noise.

The total estimated RMS noise value from the PCB and biosensor with fluid and beads in it is 73.47 mV. This noise is nearly 3 times of that obtained in simulation. During simulation, the +5V, -5V regulator circuit and on board frequency generator circuit is not considered, which contributes to extra noise. Also, interference noise from the environment is another additional source of noise not considered in our simulation. Isolating the circuit and sensor inside a metal box (faraday cage) resulted in no significant noise reduction during the measurement.

CHAPTER 4

MEASUREMENTS FOR CYTOMETRY AND RESULT ANALYSIS

4.1 Cytometry Experiment

To test the performance of the sensor and readout circuit, 1, 3 and 8 μm diameter beads were injected into the microfluidic impedance cytometer. To enable a hydrophilic channel, the bonded channel was treated with oxygen plasma. (The importance of oxygen plasma etching is discussed in appendix 7.6). Phosphate-buffered saline (PBS) was injected into the channel inlet using a micropipette. Test sample (particles and/or blood) was then pipetted in the channel. Using the hydraulic pump 11 elite diffusions dual syringe (model number 704501 from Harvard Apparatus), a steady flow of 0.08 μl/min was actuated in the fluidic channel. We used a 300 μm wide channel for testing 3 and 8 μm diameter beads. We used a 30 μm wide channel for testing solution containing 1 μm diameter beads. We simultaneously monitored the channel under an optical microscope to confirm that electrical signal changes were due to beads passing through the electrodes. The signal acquired from the PCB was recorded in LabVIEW using an NI DAQ system. The transit time for the bead to pass by the distance between two electrodes ranged between 0.13 to 0.15 s. Signal peaks had a frequency in between 6 to 8 Hz thus we used a low-pass filter cutoff of 100 Hz, the signal peaks could easily be detected. The current that was recorded from the sensor was approximately 20 nA.

Video recordings of the passage of beads through the channel were acquired to confirm that each peak indeed corresponded to the passage of beads through the electrode finger. In Fig. 4.1, we show three different positions of a single 8 µm diameter bead while passing through the electrode sensor in a 300 µm wide channel.

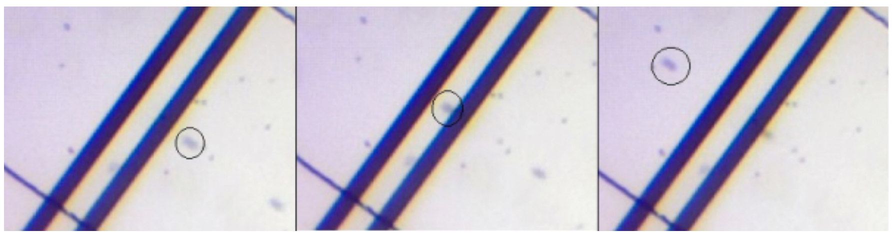

Fig. 4.1 8 µm diameter bead flow through 2 electrode sensor.

4.2 Result Analysis

In MATLAB, a Chebyshev low pass filter and wavelet de-noising technique to lower noise was used to get smooth peaks. The sample output signal corresponding to both 8 µm and 3 µm diameter bead is shown in Fig. 4.2.

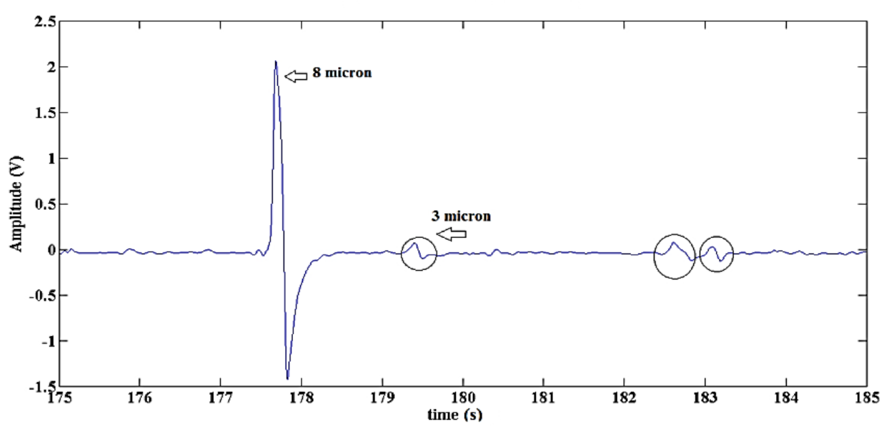

Fig. 4.2 Recorded signal after MATLAB signal analysis. Large peak is for 8 µm diameter bead and circled ones are for 3 µm diameter bead

The sample output signal corresponding to a 1 μm diameter bead is shown in Fig. 4.3.

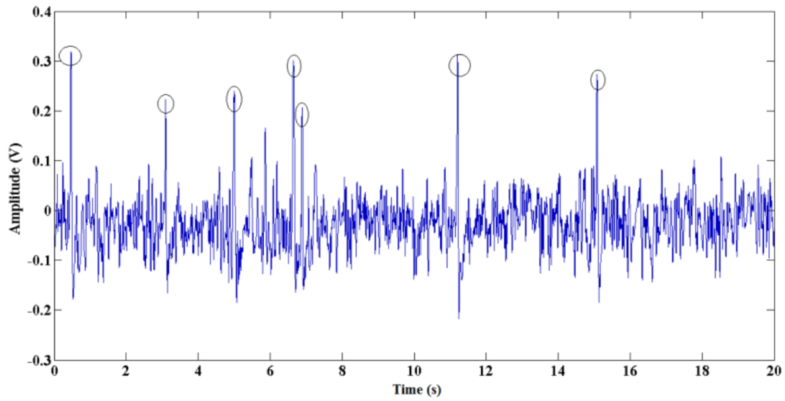

Fig. 4.3 Recorded signal after MATLAB signal analysis. Marked peaks correspond to 1 μm diameter bead

We have calculated the impedance change that the circuit can sense by taking the ratio of the spherical bead volume with respect to the active sensing channel volume. Also, SNR for different sizes of beads are calculated. For 8 μm diameter bead flow, we achieved a SNR of 184 while sensing a percentage impedance change of 0.69% in a 300 μm wide channel. We could detect 3 μm diameter beads flowing in the same channel with a SNR of 8 and a percentage impedance change of 0.032%. The SNR for a 3 μm diameter bead experiment was compared with the result from a benchtop lock-in-amplifier (Zurich Instruments HF2IS, Switzerland) and the performance was identical. We used a 30 μm wide channel to test with a 1 μm diameter bead and the SNR was 5.68. We replaced the DAQ system with a low-resolution 8 bit Arduino ADC and tested the 3 μm diameter bead in a 30 μm wide channel. The recorded SNR was 58.5.

We also computed the amplitude distribution of three different peaks. In Fig. 4.4 we show the amplitude distribution for the first experiment with 3 and 8 μm diameter bead and in Fig. 4.5 we show the result for the second experiment with 1 μm bead.

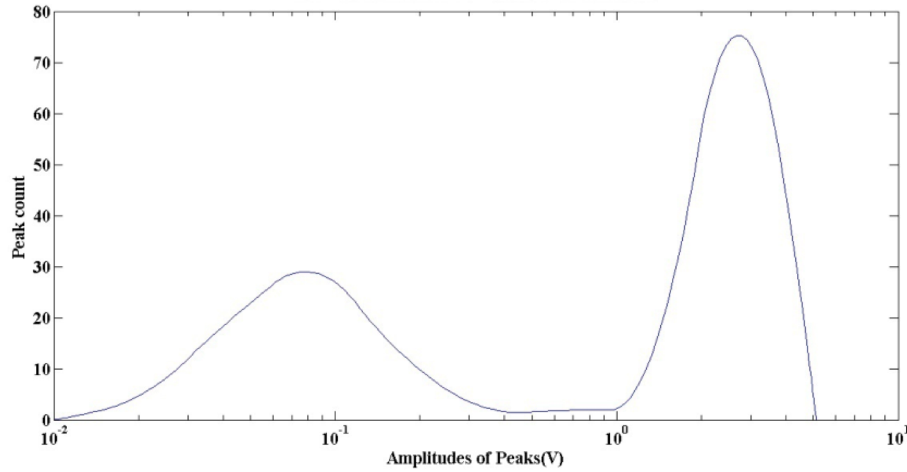

Fig. 4.4 Amplitude distribution for 3 and 8 μm diameter bead.

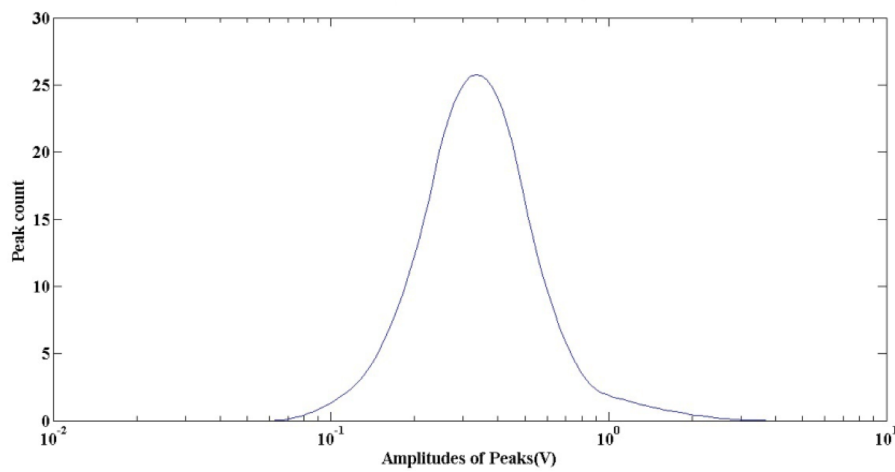

Fig. 4.5 Amplitude distribution for 1 μm diameter bead.

CHAPTER 5

REPLACING DAQ WITH MICROCONTROLLER CHIP

5.1 Experiment Result

We performed a set of experiments for 3 µm diameter beads by replacing the NI DAQ system with the 8-bit ADC from Arduino Uno. In this experiment, we used 30 µm wide channels with the identical setup as other experiments. The transit time for the 3 µm diameter bead to pass by the distance between two electrodes was between 0.08 to 0.1 s. So, signal peaks had a frequency in between 10 to 12 Hz and with a low-pass filter cutoff of 100 Hz, the signal peaks could easily get through. The recorded SNR was 58.5. In Fig. 5.1 the output signal for the 3 µm diameter bead experiment is presented and in Fig. 5.2 the amplitude distribution is presented.

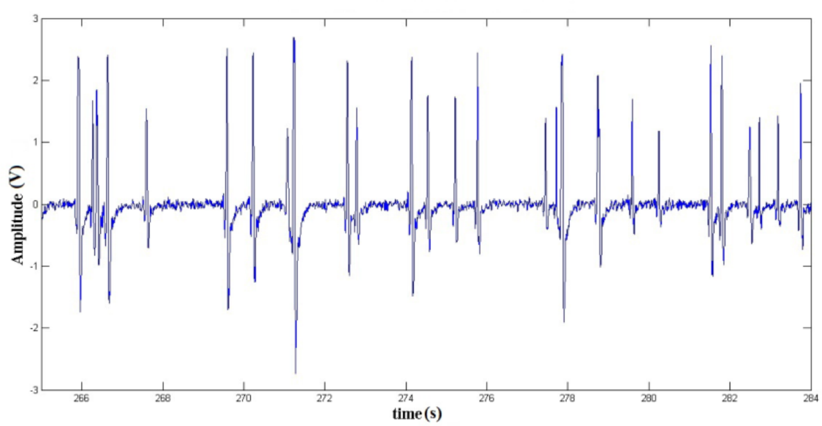

Fig. 5.1 Recorded signal after MATLAB signal analysis. 3 µm diameter bead experiment but result recorded with Arduino 8-bit ADC.

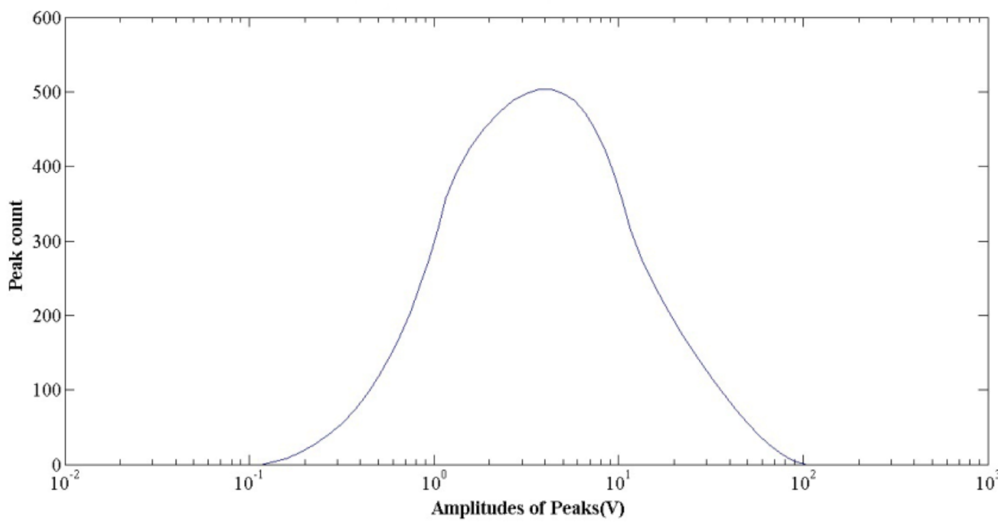

Fig. 5.2 Amplitude distribution for 3 μm diameter bead experimenting with Arduino Uno 8-bit ADC.

5.2 Result Comparison

All the results are summarized and compared with theoretical SNR predictions in Table 5.1.

TABLE 5.1: COMPARISON OF SNR AND PERCENTAGE OF BEAD VOLUME WITH RESPECT TO ACTIVE SENSING CHANNEL VOLUME FOR 1, 3, AND 8-MICROMETER DIAMETER BEAD

Bead Diameter / Channel Width Unit: Micrometer	Signal to Noise Ratio (SNR)				Percentage of Bead Volume with Respect to Active Sensing Channel Volume
	Raw	Processed	Theoretical	HF2IS Impedance Spectroscope	
1/ 30	4.34	5.68	15.71		0.12
3/ 30 With Arduino ADC	28.13	58.5	391.5		0.319
3/ 300	7.55	8.01		8.94	0.032
8/ 300	40.07	184.53			0.69

Since experimental noise measurement was three times more than the theoretical noise calculation, it was expected that the SNR from the theoretical calculation will be multiple times higher than the experimental SNR result. And in the SNR analysis, it was rightly reflected. If we consider raw SNR from the experimental result, for 1 μm diameter bead flow in a 30 μm wide channel, the theoretical SNR is nearly four times that of the experimental result. For the experiment with a 3 μm diameter bead flowing in a 30 μm wide channel and recording data with Arduino UNO AtoD, we get a SNR nearly 14 times less than theoretical SNR prediction. This anomaly can be attributed to noise contribution from the Arduino UNO and its low bit resolution and poor precision. More experiment and analysis needs to be done to testify and improve noise performance with a low-resolution AtoD. Justification for upward and downward peak signature is shown in appendix 7.8 using LTSpice simulation.

CHAPTER 6

CONCLUSION

In this work, a novel analog readout circuit is presented. We implemented the analog readout circuit for a microfluidic impedance cytometer capable of detecting particles as small as 1 µm using 8-bit data acquisition hardware. The minimum change of impedance in the sensor that we could detect was 0.032% for 3 µm diameter beads while the highest measured SNR was 184 for a 8 µm diameter bead in a 300 µm wide channel. For a 1 µm diameter bead the SNR was around 4. The SNR performance of the custom-built readout circuit for a 3 µm diameter bead experiment was comparable to a state-of-the-art bench top impedance spectrometer. We demonstrated the ability to acquire and process data using a microcontroller. The printed circuit board area for our readout circuit was 10 cm x 8 cm. Further improvements can be made by developing a fully integrated CMOS solution to further improve the detection limit and reduce the overall size and power consumption of the system, and using a standalone microcontroller instead of an entire Arduino board. We emphasize that more work is necessary to demonstrate personalized health monitoring including integration of miniaturized fluidic pumping, specialized packaging for a robust and rugged interface, mechanisms for device failure mitigation and detection, along with on-chip sample preparation depending on the application of interest. In this study, our goal was to show the potential of moving towards personalized health monitoring through the combination of electronic biosensors, with no compromise in performance compared to state-of-the-art benchtop electronic measurement and data acquisition systems.

CHAPTER 7

APPENDIX

7.1 Signal Analysis in Lock-in Amplification Process

We used a high-frequency reference voltage signal v_{ref} to modulate low-frequency current generation created by the bead flow in the sensor. The equation of this signal is:

$$v_{ref} = V_{in} \sin\left(\omega_{ref} t + \Theta_{ref}\right) \quad \ldots\ldots \quad (7.1)$$

Where, V_{in} is amplitude of reference signal, ω_{ref} is frequency of reference signal in radian/sec, and Θ_{ref} is phase of the reference signal in radian.

This reference signal is passed in the biosensor. The current signal which comes out of the sensor can be approximated as:

$$i_{sensor} = I_{sig} \sin\left(\omega_{ref} t + \Theta_{sig} + \Theta_{ref}\right) \quad \ldots\ldots \quad (7.2)$$

Where, I_{sig} is amplitude of sensor current output, Θ_{sig} is the phase of the current signal introduced in the sensor.

The trans-impedance amplifier introduces a 180° phase shift to the input signal. At the output of the trans-impedance amplifier we obtain,

$$v_{TIA} = V_{TIA} \sin\left(\omega_{ref} t + \Theta_{sig} + \Theta_{ref} + 180°\right) \quad \ldots\ldots \quad (7.3)$$

$$V_{TIA} = I_{sig} R_{TIA-fb} \quad \ldots\ldots \quad (7.4)$$

Where, R_{TIA-fb} is feedback resistance of the trans-impedance amplifier, and V_{TIA} is the output voltage amplitude of the trans-impedance amplifier.

When this signal is passed through the analog multiplier, it is multiplied with a reference signal which is shifted by 180°. We obtain at the output of the mixer

$$v_{mixer} = V_{TIA} \sin\left(\omega_{ref} t + \Theta_{sig} + \Theta_{ref} + 180°\right) V_{in} \sin\left(\omega_{ref} t + +\Theta_{ref} + 180°\right) \quad (7.5)$$

$$\Leftrightarrow v_{mixer} = \frac{1}{2} V_{TIA} V_{in} \left\{\cos \Theta_{sig} - \cos\left(2\omega_{ref} t + \Theta_{sig} + 2\Theta_{ref}\right)\right\} \quad (7.6)$$

At the output of the low pass filter stage, the high frequency $(2\omega_{ref})$ component will be filtered out so that the only remaining part is

$$v_{lpf} = \frac{1}{2} V_{TIA} V_{in} \cos \Theta_{sig} \quad (7.7)$$

When a bead passes through the microfluidic channel, amplitude modulation occurs in the sensor and the current coming out of the sensor is found to be

$$i_{exp} = I_{sig}[1 + mx(t)] \sin\left(\omega_{ref} t + \Theta_{sig}\right) \quad (7.8)$$

Where, I_{sig} is the amplitude of the current signal, m is the modulation index and, $x(t)$ is time varying signal introduced by crossing of bead through electrode sensor.

Eventually, at the output of the low pass filter stage we obtain

$$v_{lpf} = \frac{1}{2} V_{TIA} V_{in} [1 + mx(t)] \cos \Theta_{sig} \quad (7.9)$$

A dc blocking capacitor is used as high pass filter to block the dc component of this signal. So, at the output of the capacitor, we obtain

$$v_{cap} = \frac{1}{2} V_{TIA} V_{in} mx(t) \cos \Theta_{sig} \quad (7.10)$$

This signal does not depend on the phase matching between the reference signal and the current coming out of the sensor.

7.2 Resistance Calculation for Base Electrolyte Solution

Gerwen et al. showed an elliptical model of current comprisement of inter-digitated electrodes [30]. This model is reproduced in MATLAB and is shown in Fig. 7.1. According to the height of the channel, certain current conduction paths get clipped which limits the resistance value of the channel solution. Using this model, the base fluid resistances corresponding to different channel heights are calculated. For a channel height of 10 μm the solution, resistance is 214210 Ω.

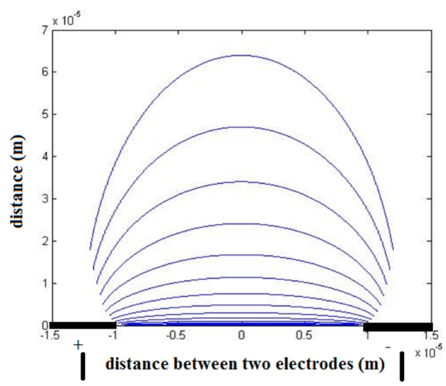

Fig. 7.1. Current conduction paths between two electrodes.

7.3 Method of Calculation for Current Variation (ΔI) in the Biosensor

Since channel length is longer than its diameter, a method by Deblois and Bean can be used to approximate the increase in resistance of a circular cylindrical conducting channel [32].

$$r \cong -\left(\frac{4\rho d^3}{\pi {D_m}^4}\right) \quad (7.11)$$

$$\Delta I \cong Abs\left(\frac{r}{R^2}\right) * V_{in} \quad (7.12)$$

Where, r is the approximate increase in resistance of a circular cylindrical conducting channel, ρ is the resistivity of the electrolyte, d is the diameter of the passing bead, D_m is the diameter of the cylindrical channel, ΔI is the current variation introduced by bead flow in the channel, R is the resistance of the electrolyte, and V_{in} is the input reference voltage signal amplitude.

7.4 SNR Calculation Method

The SNR is calculated using the equation

$$SNR = \frac{Voltage\ peak}{\sqrt{(noise\ variance)}} \quad (7.13)$$

To calculate voltage peak, mean for all the output signal peaks are calculated in MATLAB.

7.5 Different Blocks in Lock-in Amplifier Circuit

7.5.1 Voltage Regulator Circuit

We have used AD835 Analog Multiplier IC as mixer which has a power supply voltage requirement of ±5V. The trans-impedance amplifier TL071 also operates well with this power supply range. We have used two 9V lithium ion rechargeable batteries as power supply. To get ±5V from two 9V batteries, we need a +5V and a -5V voltage regulator.

Since this is high-frequency circuit operation, power supply stability and low noise performance are major concerns when choosing voltage regulators. We picked the LT1763 voltage regulator which gives +5V at the output and provides a highest current of 500 mA with low noise 20 μV_{rms} (for frequency range of 10Hz to 100 kHz). The LT1763 IC comes in SOIC package, so a SOIC to DIP adapter socket is used to mount the IC on the PCB. The circuit for the +5V voltage regulator is shown in Fig 7.2.

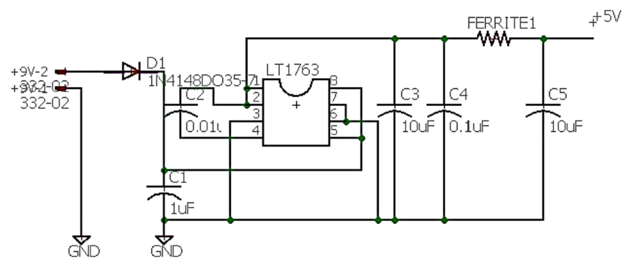

Fig 7.2. +5V voltage regulator

We picked the LT1964 voltage regulator which gives -5V at the output and provides a highest possible current of 200 mA with low noise 30 μV_{rms} (for frequency range of 10Hz to 100 kHz). The LT1964 IC comes in 5 lead SOT-23 package, so we used a SOT-23 to 8DIP adapter socket to mount the IC on the PCB. The circuit for -5V voltage regulator is shown in Fig 7.3.

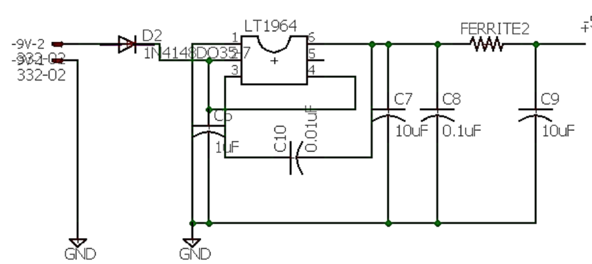

Fig 7.3. -5V voltage regulator

7.5.2 Power Supply Noise Reduction

Power supply noise reduction is crucial which is done using circuit bypassing and decoupling techniques. Voltage regulators have finite bandwidth so output impedance increases with frequency. The voltage regulator can be modeled as a stray inductance in series with the load impedance. At high frequency, this inductance adding with other lead inductances introduces significant resistance value which causes noise voltage fluctuation. This voltage fluctuation can cause problems for circuit operations. To reduce noise voltage fluctuation, bypassing capacitors are used. A capacitor which filters out an AC signal by removing the noise and provides a DC signal, is called a bypass capacitor. Different size capacitors are used across output voltage to reduce different noise frequency components. For low-frequency noise rejection a large size capacitor is needed (we used 10 μF) and for the high-frequency noise rejection a small size capacitor is needed (we used 0.1 μF). The bypassing capacitor introduces a low impedance path for noise fluctuation, thus reducing noise fluctuation due to stray inductance. Also, bypassing capacitors need to be connected closer to the power supply pin for each IC. It is because larger traces on PCBs can introduce series inductance thus degrading the performance of bypass capacitors.

For decoupling, a ferrite bead is used as a high impedance element in series with the power supply line. This causes circuit isolation so that noise fluctuation cannot transmit through the circuit. It also assists to the noise signal bypassing, making sure that noise current will flow through the low impedance bypass capacitor. However, with the higher inductance of the ferrite bead, there is a chance of high noise voltage fluctuation at the output of voltage regulator. The smallest size of an inductor that does the job of circuit isolation should therefore be used.

7.5.3 Signal Generator Circuit

Our LIA design consists of an onboard single frequency (500 kHz) function generator. The signal generator circuit is shown in Fig. 7.4.

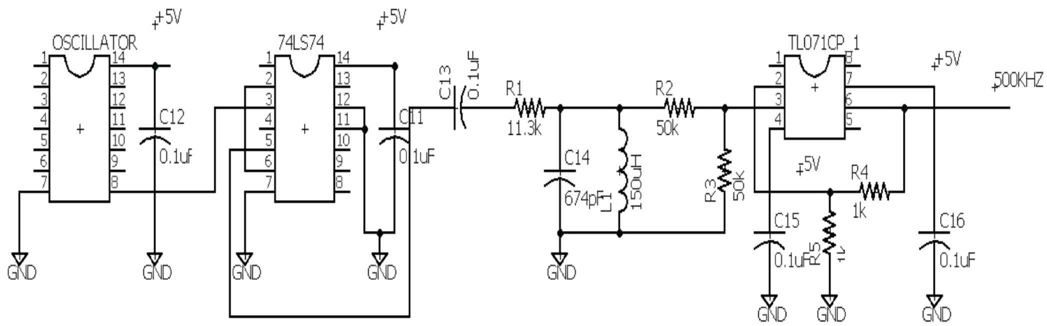

Fig 7.4. Signal Generator Circuit

To produce a $2V_{p\text{-}p}$ 500 kHz sine wave, we used a 1 MHz crystal oscillator ECS-100AC which gives a $5V_{p\text{-}p}$ square wave. A 0.1 µF is used to remove the dc offset of the square wave. A flipflop IC 74LS74 is used to divide the signal frequency by two. A passive LC tank is used to remove all frequency components except 500 kHz. The center of the band is at 500 kHz, so it rejects all other frequencies and gives a smooth sine wave signal. The spectrum of the band pass passive LC filter tank is shown in Fig. 7.5.

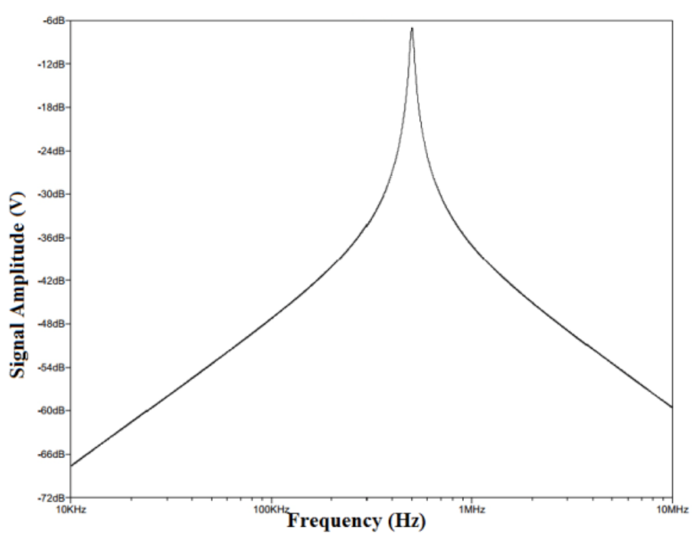

Fig. 7.5.Gain versus frequency plot for passive LC tank. Center of band is at 500 kHz.

A TL071 operational amplifier is used to provide a steady $2V_{p-p}$ sine wave with a 500 kHz frequency at its output and to avoid loading effect. The input signal has a resolution of 20 mV.

7.5.4 Operational Amplifier Oscillation

Special care is needed to avoid self-oscillation problem of operational amplifier. If internal compensation circuitry is absent in high-speed operational amplifier, a high-value resistor used in the feedback path can cause self-oscillation regardless of input voltage. We started our design with the AD8067 IC which has extremely low noise and high bandwidth. But it does not have internal compensation circuitry to counter self-oscillation. Also, resistor values more than 1 kΩ could not be used in the feedback path of this opamp. We replaced this opamp with ADA4817 which does not have a restriction on the feedback resistor, but still it does not have internal compensation circuitry. Early experiments were performed on the breadboard, where breadboard holes introduced some inductance. With high operating frequency this inductance introduces considerable impedance. This impedance made a path for the output return to the input side and created a feedback loop, thus causing oscillation. Also, noise fluctuation in the supply voltage aggravated the situation. Using a 0.5 to 1pF capacitor across the feedback path can reduce this oscillation. High inverting gain stages also suffers from amplified internal noise of the operational amplifier, which aggravates the noise performance of the circuit. Using a 0.5 pF in the feedback path of the operational amplifier makes it a low pass filter and suppresses high-frequency noise.

However, we later switched to a low noise general purpose operational amplifier TL071 which has noise of 18 nV/√Hz at f=1 kHz and has internal compensation circuitry. With this operational amplifier, we were able to eliminate the self-oscillation problem.

7.5.5 Third-Order Butterworth LPF

For the low pass filter, we have cascaded a second order active Butterworth low pass filter with one order passive low pass filter to get third order low pass filter. The cutoff frequency of the low-pass filter is 102 Hz. The low pass filter circuit is shown in figure 7.6.

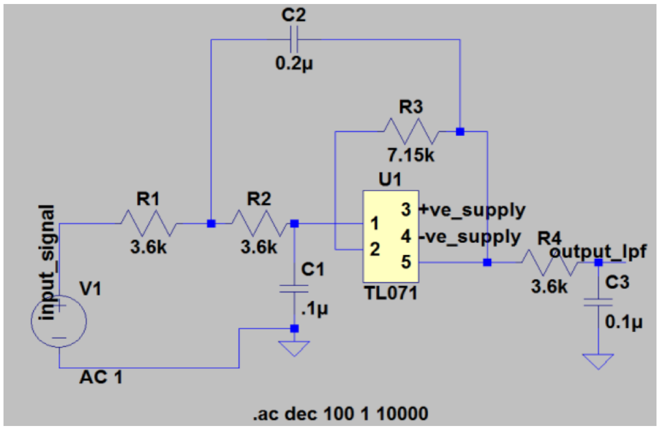

Fig 7.6. Third-order Butterworth LPF (cutoff 102 Hz)

The motivation for using third order Butterworth low pass filter is to get a 60 dB roll-off for better high-frequency noise rejection. The AC response of the LPF circuit, between 1 Hz to 10 kHz, is shown in Fig. 7.7. Signal amplitude rolls down to -81 dB at 10 kHz frequency and the phase is above -180° within our frequency range of interest.

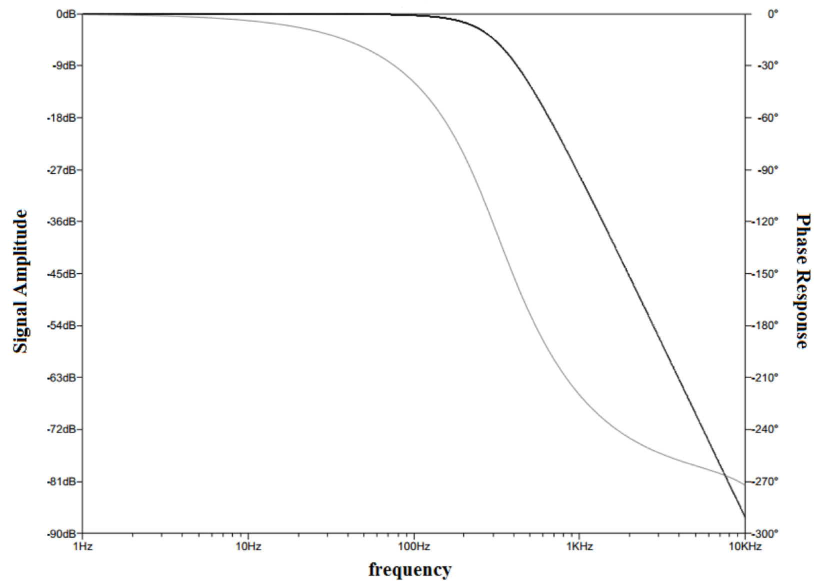

Fig. 7.7. AC Response of third-order Butterworth LPF. Bold line is magnitude response and opaque line is phase response.

7.5.6. LTSpice Noise Simulation

Noise simulation is performed in LTSpice IV software. The circuit for noise simulation is shown in Fig. 7.8.

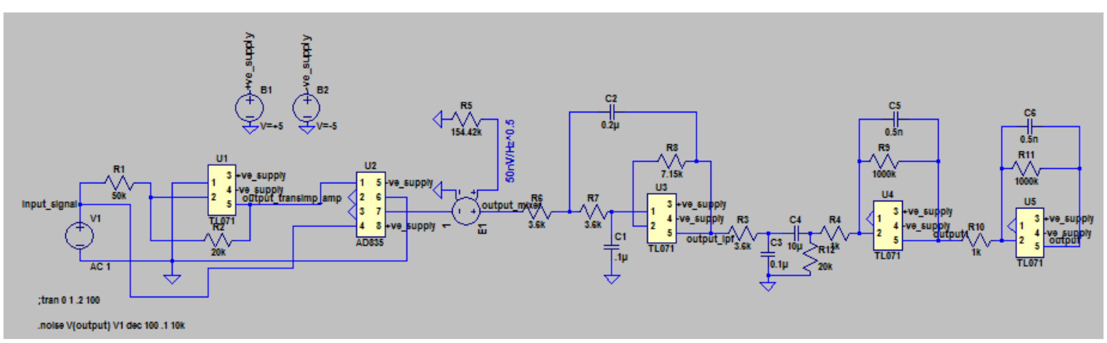

Fig. 7.8. Noise simulation circuit

For the trans-impedance amplifier, we have used the TL071 spice model from Texas Instruments website. For the analog mixer chip AD835, the model that we used does not contain noise information. Therefore, we had to externally add a 50 nV/√Hz voltage source at the output to simulate its noise. However, none of the IC models contain flicker noise information, so we could not simulate flicker noise in the theoretical noise calculation.

7.5.7. Noise Suppression in High Gain Stages

The TL071 opamp was used to build an inverting high gain stage which provides a gain of 1000. This high gain also amplifies the internal noise of the opamp, which aggravates the noise performance of the circuit. To suppress this noise, a 0.5 nF capacitor is placed across the feedback resistor. So the opamp now works as low pass filter and suppresses high-frequency noise. In Fig. 7.9, overall circuit noise without high gain stage noise suppression is presented.

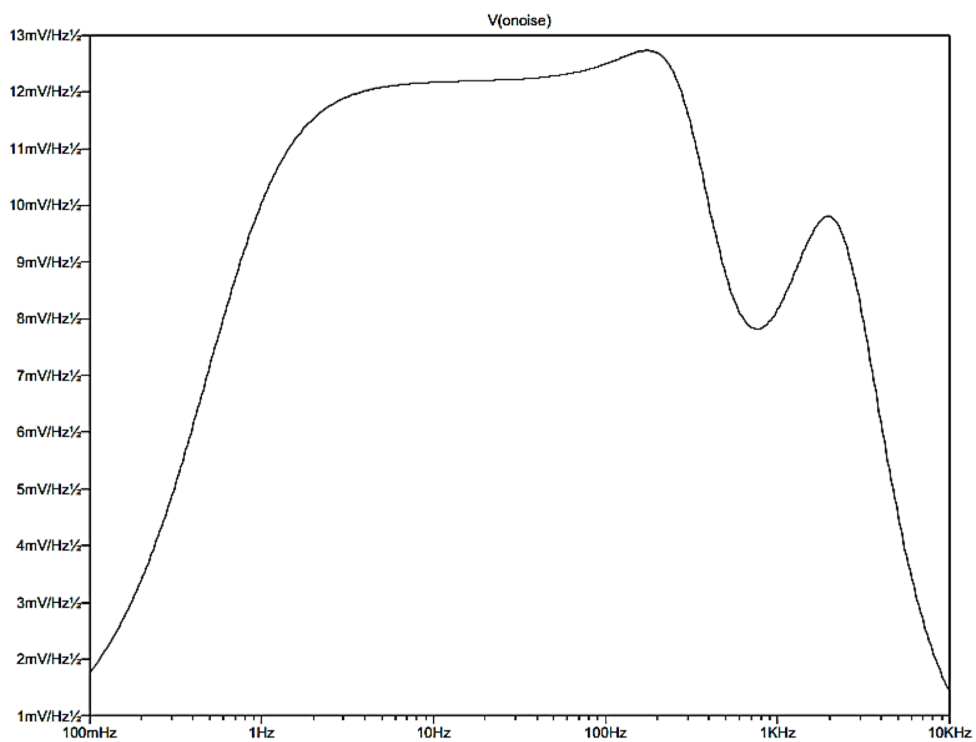

Fig 7.9. Noise simulation without high gain stage noise suppression

7.5.8 Layout Design Board Planes

For designing the PCB, we have used Eagle CAD software. In Fig. 7.10 the bottom plane of the PCB is shown. Traces are shown on the bottom plane. In Fig. 7.11 the top plane of the PCB is shown. Four mounting holes are placed on four corners of the board.

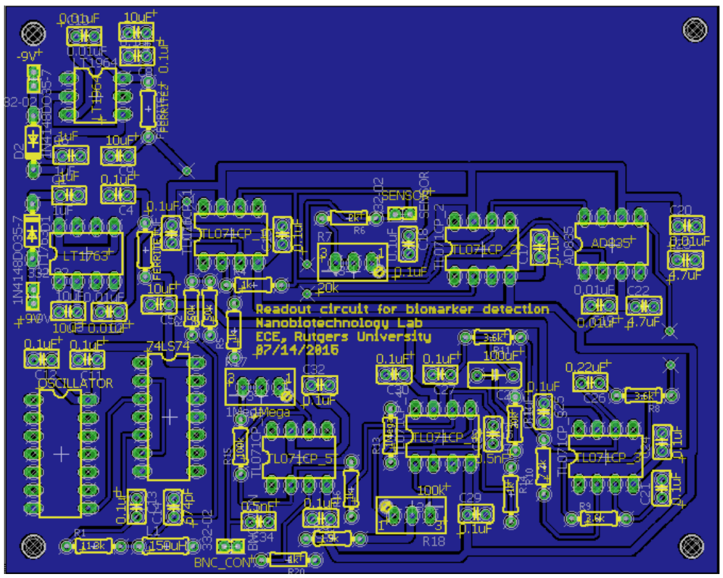

Fig. 7.10. PCB bottom plane

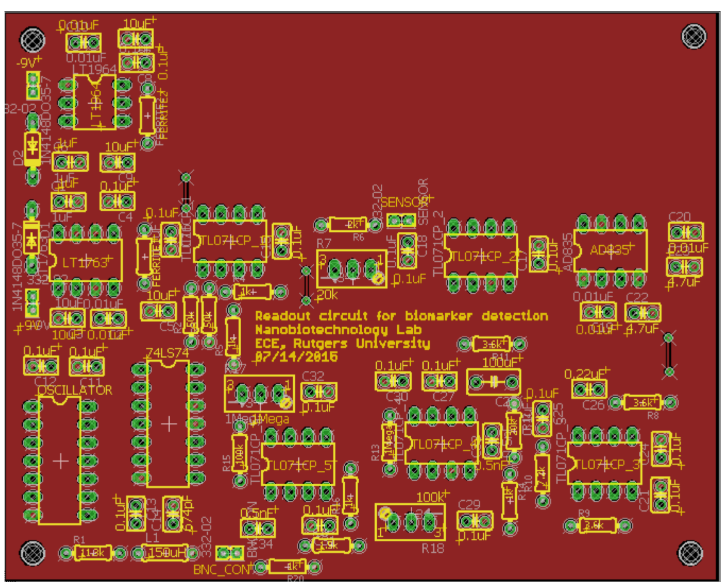

Fig. 7.11. PCB top plane

The ground plane is common to both planes which reduces cross talk and interference noise between traces. Also, the voltage drop due to the ground trace is avoided so the ground potential is the same in all ground pins. Power traces carry a larger amount of current than normal traces, so they are wider than normal traces.

7.6 Oxygen Plasma Etching

Oxygen plasma treatment on PDMS changes its surface properties from hydrophobic to hydrophilic [33]. Intrinsically, PDMS is hydrophobic making it difficult to wet the microchannel. The polar function group sialons makes the surface of the microchannel hydrophilic.

7.7 Arduino UNO

Arduino UNO is a microcontroller board based on ATMega328. It provides a built-in 10-bit ADC. We used this board as a AtoD replacing our DAQ measurement. The output digital signal coming out of the Arduino board was reconstructed in Arduino 1.6.3 software and then recorded using Processing 3 software (processing.org). The Arduino UNO module is shown in figure 7.12.

Fig 7.12. Arduino UNO Rev3

7.8 Justification for Upward-downward Peak Signature

When a bead passes through the two electrodes, the current decreases, causing an increase in voltage due to a 180-degree phase shift introduced by the trans-impedance amplifier. The output of the low pass filter stage is a sharp positive peak with a baseline that drifts over time. The DC blocking capacitor removes the baseline; however, it adds a negative overshoot. If we consider a sharp positive half sine wave peak at the input of the capacitor, for the input positive edge, the output rises sharply, while for the negative edge of the input, the output falls sharply and then tries to recover with time. This small negative overshoot is greatly amplified by two high gain stages and ends up as a signature positive peak followed by a negative peak at the output of the circuit. The phenomenon was also verified using LTSpice IV. The output of the second inverting gain stage in LTSpice is shown in Fig. 7.13 which is identical in shape to our experimental result.

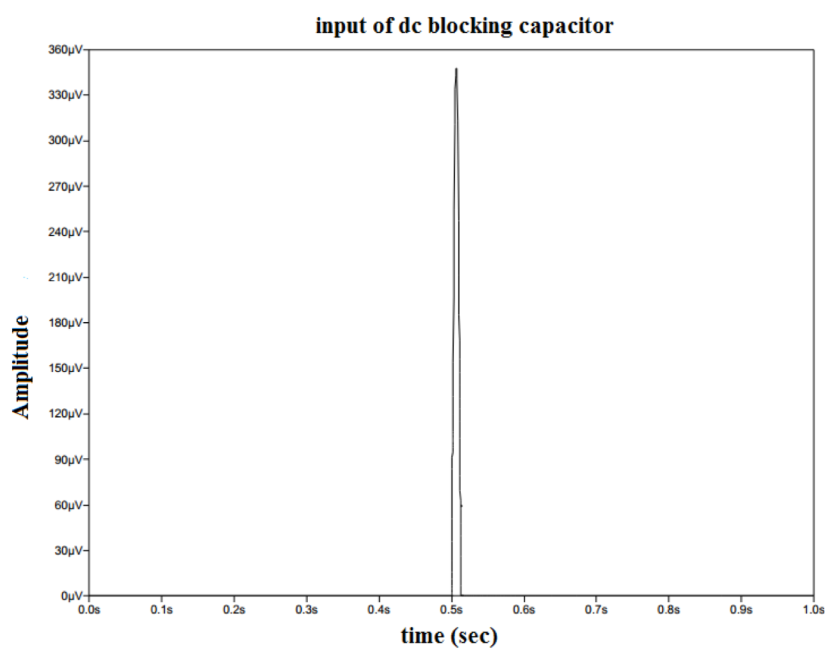

(a)

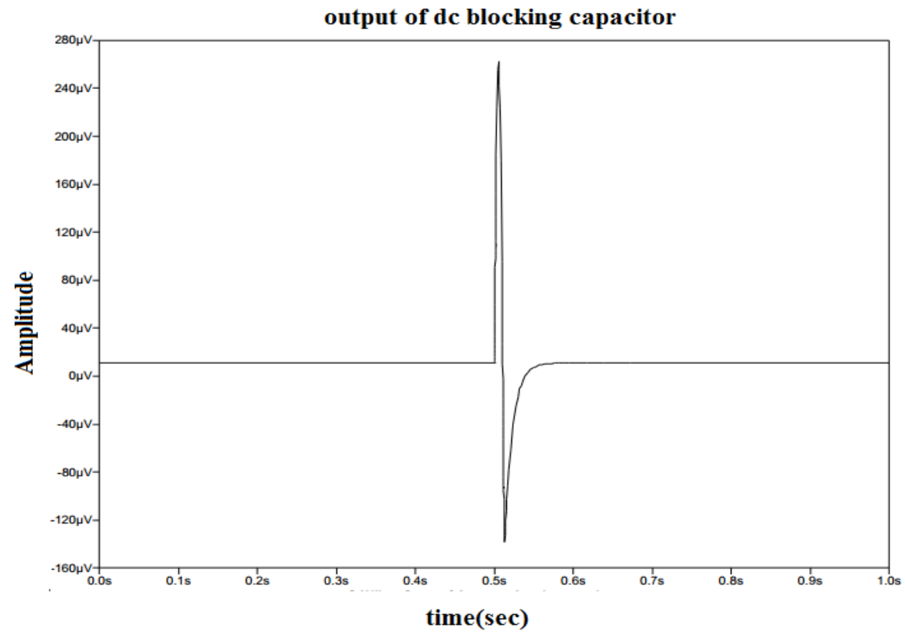
output of dc blocking capacitor
280µV
240µV
200µV
160µV
120µV
80µV
40µV
0µV
-40µV
-80µV
-120µV
-160µV
Amplitude
0.0s
0.1s
0.2s
0.3s
0.4s
0.5s
0.6s
0.7s
0.8s
0.9s
1.0s
time(sec)

(b)

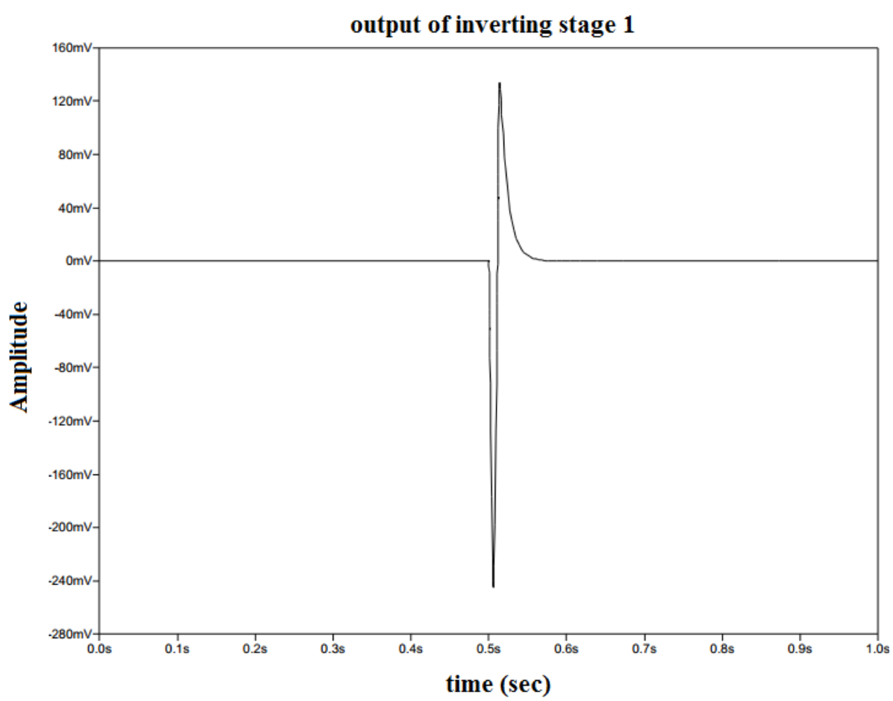
output of inverting stage 1
160mV
120mV
80mV
40mV
0mV
-40mV
-80mV
-120mV
-160mV
-200mV
-240mV
-280mV
Amplitude
0.0s
0.1s
0.2s
0.3s
0.4s
0.5s
0.6s
0.7s
0.8s
0.9s
1.0s
time (sec)

(c)

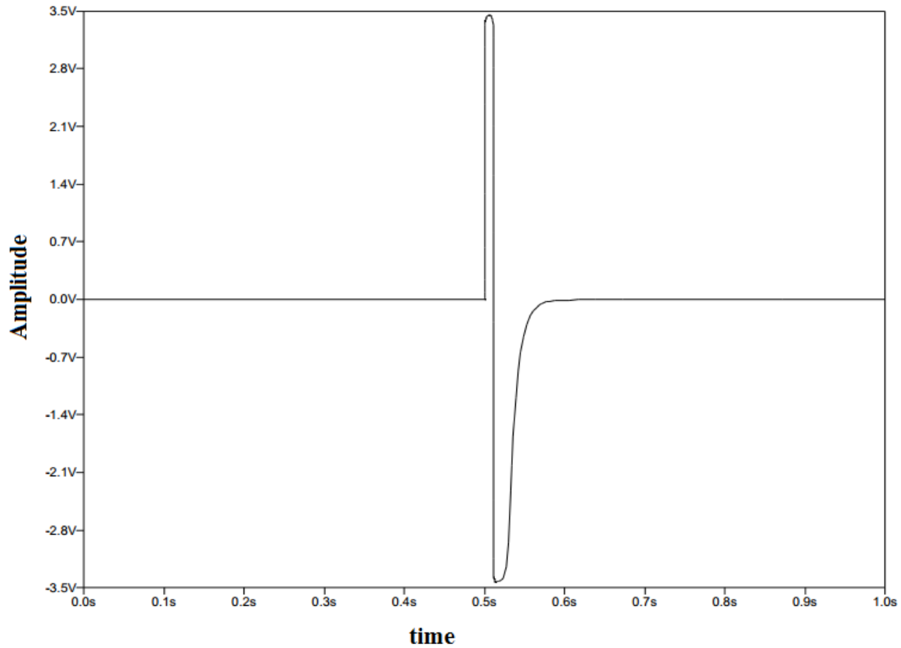

(d)

Fig. 7.13. Simulation result to justify the nature of peak. (a) input of dc blocking capacitor, (b) output of dc blocking capacitor, (c) output of first inverting gain stage, (d) output of second inverting gain stage.

Bibliography

[1] S. Emaminejad, K. Paik, V. Tabard-Cossa, and M. Javanmard, “Portable Cytometry Using Microscale Electronic Sensing,” *Sensors Actuators B. Chem.*, 2015.

[2] S. Emaminejad, M. Javanmard, R. W. Dutton, and R. W. Davis, “Microfluidic diagnostic tool for the developing world: contactless impedance flow cytometry,” *Lab Chip*, vol. 12, no. 21, pp. 4499–4507, 2012.

[3] A. Sun, T. Wambach, A. G. Venkatesh, and D. A. Hall, “A Low-Cost Smartphone-Based Electrochemical Biosensor for Point-of-Care Diagnostics,” no. Cv, pp. 14–17, 2014.

[4] J. Jiang, X. Wang, R. Chao, Y. Ren, C. Hu, Z. Xu, and G. Logan, “Sensors and Actuators B : Chemical Smartphone based portable bacteria pre-concentrating microfluidic sensor and impedance sensing system,” *Sensors Actuators B. Chem.*, vol. 193, no. 2014, pp. 653–659, 2016.

[5] T.. Wilmshurst, *Signal Recovery from Noise in Electronic Instrumentation*, 2nd ed. Taylor&Francis Group, New York, NY, USA, 1990.

[6] S. R. Systems, “About Lock-In Amplifiers, Application Note #3,” 1999.

[7] J. Lichtenberg, N. F. de Rooij, and E. Verpoorte, “A microchip electrophoresis system with integrated in plane electrodes for contactless conductivity detection,” *Electrophoresis*, vol. 23, no. 21, pp. 3769–3780, 2002.

[8] M. Gabal, N. Medrano, B. Calvo, P. A. Martínez, S. Celma, and M. R. Valero, “A complete low voltage analog lock-in amplifier to recover sensor signals buried in noise for embedded applications,” *Procedia Eng.*, vol. 5, pp. 74–77, 2010.

[9] A. De Marcellis, G. Ferri, and P. Mantenuto, “A New Single-Chip Analog Lock-In

Amplifier with Automatic Phase and Frequency Tuning for Physical/Chemical Noisy Phenomena Detection," pp. 121–124, 2013.

[10] T. Sun, D. Holmes, S. Gawad, N. G. Green, and H. Morgan, "High speed multi-frequency impedance analysis of single particles in a microfluidic cytometer using maximum length sequences {," pp. 1034–1040, 2007.

[11] M. O. Sonnaillon and F. J. Bonetto, "of measuring multiple frequencies sweeps simultaneously A low-cost , high-performance , digital signal processor-based lock-in amplifier capable of measuring multiple frequency sweeps simultaneously," vol. 024703, no. 2005, pp. 0–7, 2015.

[12] C. Yang, D. Rairigh, and A. Mason, "Fully Integrated Impedance Spectroscopy Systems for Biochemical Sensor Array," pp. 21–24, 2007.

[13] C. Yang, S. R. Jadhav, R. M. Worden, A. J. Mason, S. Member, and I. Terms, "Compact Low-Power Impedance-to-Digital Converter for Sensor Array Microsystems," vol. 44, no. 10, pp. 2844–2855, 2009.

[14] F. C. Bo Ye Ming Li, "The Digital Lock-in Amplifier for Detecting the Power Traveling Wave Signal TT -," *Int. J. Signal Process. Image Process. Pattern Recognit.*, vol. 8, no. 4, pp. 361–374, Apr. 2015.

[15] L. E. Bengtsson, "A microcontroller-based lock-in amplifier for sub-milliohm resistance measurements," vol. 075103, pp. 1–8, 2012.

[16] Z. Instruments, "HF2IS Impedance Spectroscope." [Online]. Available: https://www.zhinst.com/products/hf2is.

[17] FEMTO, "Single Board Lock-in Amplifier Series LIA-BVD 150 H 19'' board." [Online].

Available: http://www.femto.de/en/products/lock-in-amplifiers/single-board-series-lia-bv-150.html.

[18] U. Marschner, H. Grätz, B. Jettkant, D. Ruwisch, G. Woldt, W. Fischer, and B. Clasbrummel, “Sensors and Actuators A : Physical Integration of a wireless lock-in measurement of hip prosthesis vibrations for loosening detection,” vol. 156, pp. 145–154, 2009.

[19] A. Gnudi, L. Colalongo, G. Baccarani, U. Bologna, and M. Risorgimento, “Integrated Lock-In Amplifier for Sensor Applications,” pp. 58–61.

[20] C. Azzolini, A. Magnanini, M. Tonelli, G. Chiorboli, and C. Morandi, “Integrated Lock-In Amplifier for Contactless Interface to Magnetically Stimulated Mechanical Resonators,” 2008.

[21] A. D. Amico, A. De Marcellis, C. Di Carlo, C. Di Natale, G. Ferri, E. Martinelli, R. Paolesse, and V. Stornelli, “Sensors and Actuators B : Chemical Low-voltage low-power integrated analog lock-in amplifier for gas sensor applications,” *Sensors Actuators B. Chem.*, vol. 144, no. 2, pp. 400–406, 2010.

[22] K.-H. Lee, J. Nam, S. Choi, H. Lim, S. Shin, and G.-H. Cho, “A CMOS impedance cytometer for 3D flowing single-cell real-time analysis with ΔΣ error correction,” in *Solid-State Circuits Conference Digest of Technical Papers (ISSCC), 2012 IEEE International*, 2012, pp. 304–306.

[23] A. Manickam, C. A. Johnson, S. Kavusi, and A. Hassibi, “Interface design for CMOS-integrated electrochemical impedance spectroscopy (EIS) biosensors,” *Sensors*, vol. 12, no. 11, pp. 14467–14488, 2012.

[24] P. Kassanos, I. F. Triantis, and A. Demosthenous, “A CMOS magnitude/phase

measurement chip for impedance spectroscopy," *Sensors Journal, IEEE*, vol. 13, no. 6, pp. 2229–2236, 2013.

[25] P. Kassanos, L. Constantinou, I. F. Triantis, and A. Demosthenous, "An integrated analog readout for multi-frequency bioimpedance measurements," *Sensors Journal, IEEE*, vol. 14, no. 8, pp. 2792–2800, 2014.

[26] P. Murali, I. Izyumin, D. Cohen, J.-C. Chien, A. M. Niknejad, and B. Boser, "24.6 A CMOS micro-flow cytometer for magnetic label detection and classification," in *Solid-State Circuits Conference Digest of Technical Papers (ISSCC), 2014 IEEE International*, 2014, pp. 422–423.

[27] H. Huang and S. Palermo, "A TDC-Based Front-End for Rapid Impedance Spectroscopy," no. 1, pp. 169–172, 2013.

[28] P. M. Maya-hernández, L. C. Álvarez-simón, M. T. Sanz-Pascual, and B. Calvo-lópez, "An Integrated Low-Power Lock-In Amplifier and Its Application to Gas Detection," pp. 15880–15899, 2014.

[29] J. Gu and N. Mcfarlane, "A Low Power Multi-Frequency Current Mode Lock-in Amplifier for Impedance Sensing," pp. 6–11, 2015.

[30] P. Van Gerwen, W. Laureys, G. Huyberechts, M. Op De Beeck, K. Baert, J. Suls, A. Varlan, W. Sansen, L. Hermans, and R. Mertens, "NANOSCALED INTERDIGITATED ELECTRODE ARRAYS FOR BIOCHEMICAL SENSORS," pp. 907–910, 1997.

[31] T. Instruments, "PCB design guidelines for reduced EMI," 1999. [Online]. Available: http://www.ti.com/lit/an/szza009/szza009.pdf.

[32] R. W. Deblois and C. P. Bean, "Counting and Sizing of Submicron Particles by the

Resistive Pulse Technique," vol. 909, no. 1970, 1995.

[33] S. H. Tan, N. Nguyen, and C. Chua, "Oxygen plasma treatment for reducing hydrophobicity of a sealed polydimethylsiloxane microchannel," pp. 1–9, 2010.